


Phosphoproteomic analysis of lung tissue from patients with pulmonary arterial hypertension

Ravikumar Sitapara¹, TuKiet T. Lam^{2,3}, Aneta Gandjeva⁴, Rubin M. Tuder⁴ and Lawrence S. Zisman^{1,5} 

¹Rensselaer Center for Translational Research Inc., Troy, NY, USA; ²Department of Molecular Biophysics and Biochemistry, Yale University, Yale University, New Haven, CT, USA; ³MS & Proteomics Resource, WM Keck Foundation Biotechnology Resource Laboratory, Yale University, New Haven, CT, USA; ⁴Program in Translational Lung Research, Division of Pulmonary Sciences and Critical Care Medicine, University of Colorado School of Medicine, Aurora, CO, USA; ⁵Pulmokine Inc., Troy, NY, USA

Abstract

Pulmonary arterial hypertension (PAH) is a rare disorder associated with high morbidity and mortality despite currently available treatments. We compared the phosphoproteome of lung tissue from subjects with idiopathic PAH (iPAH) obtained at the time of lung transplant with control lung tissue. The mass spectrometry-based analysis found 60,428 phosphopeptide features from which 6622 proteins were identified. Within the subset of identified proteins there were 1234 phosphopeptides with $q < 0.05$, many of which are involved in immune regulation, angiogenesis, and cell proliferation. Most notably there was a marked relative increase in phosphorylated (S378) IKZF3 (Aiolos), a zinc finger transcription factor that plays a key role in lymphocyte regulation. In vitro phosphorylation assays indicated that GSK3 alpha and/or GSK3 beta could phosphorylate IKZF3 at S378. Western blot analysis demonstrated increased pIKZF3 in iPAH lungs compared to controls. Immunohistochemistry demonstrated phosphorylated IKZF3 in lymphocytes surrounding severely hypertrophied pulmonary arterioles. In situ hybridization showed gene expression in lymphocyte aggregates in PAH samples. A BCL2 reporter assay showed that IKZF3 increased BCL2 promoter activity and demonstrated the potential role of phosphorylation of IKZF3 in the regulation of BCL mediated transcription. Kinase network analysis demonstrated potentially important regulatory roles of casein kinase 2, cyclin-dependent kinase I (CDK1), mitogen-associated protein kinases (MAPKs), and protein kinases (PRKs) in iPAH. Bioinformatic analysis demonstrated enrichment of RhoGTPase signaling and the potential importance of cGMP-dependent protein kinase I (PRKG). In conclusion, this unbiased phosphoproteomic analysis demonstrated several novel targets regulated by kinase networks in iPAH, and reinforced the potential role of immune regulation in the pathogenesis of iPAH. The identified up- and down-regulated phosphoproteins have potential to serve as biomarkers for PAH and to provide new insights for therapeutic strategies.

Keywords

pulmonary hypertension, proteomics, cell proliferation/cell cycle, angiogenesis, inflammation

Date received: 25 July 2020; accepted: 18 June 2021

Pulmonary Circulation 2021; 11(3) 1–15

DOI: 10.1177/20458940211031109

Introduction

Pulmonary arterial hypertension (PAH) is a rare disorder of the pulmonary vasculature associated with high morbidity and mortality. The pathology of the disease includes both plexiform lesions of disorganized angiogenesis, and abnormal neointimal cellular proliferation which obstructs blood flow through the pulmonary arterioles.^{1–7} Several transcriptional and proteomic analyses have been performed in PAH

samples; because lung biopsy is relatively contraindicated in PAH, the preponderance of these studies have been in circulating cells and blood.^{8–19} The few studies performed on

Corresponding author:

Lawrence S. Zisman, Pulmokine Inc., 105 Jordan Road, Ste 3 Troy, NY 12180, USA.

Email: lz@pulmokine.net



Creative Commons Non Commercial CC BY-NC: This article is distributed under the terms of the Creative Commons Attribution-NonCommercial 4.0 License (<https://creativecommons.org/licenses/by-nc/4.0/>) which permits non-commercial use, reproduction and distribution of the work without further permission provided the original work is attributed as specified on the SAGE and Open Access pages (<https://us.sagepub.com/en-us/nam/open-access-at-sage>).

© The Author(s) 2021
Article reuse guidelines:
sagepub.com/journals-permissions
journals.sagepub.com/home/pul



lung tissue have relied on samples obtained at the time of lung transplant.^{17,18} In general, these studies have found that pathways involved in immune system control, vascular biology, and cell proliferation are highly regulated in PAH. However, recent attempts to find overlap between targets regulated at the level of gene expression in circulating cells and lung resident cells implicated in PAH pathobiology are somewhat more problematic, yielding few points of intersection.^{11,17} Single cell RNA sequencing of PAH lung according to specific cell types may provide incremental information compared to whole tissue transcriptomics.¹⁸ The vast majority of proteomic studies in PAH have looked solely at total protein in the compartment of interest (such as plasma, blood outgrowth endothelial cells, or transformed lymphocytes).^{9,10,12,16} Xu et al.¹⁵ performed both a proteomic and phosphoproteomic analysis in pulmonary arterial endothelial cells cultured from human PAH lungs obtained at the time of lung transplant. To our knowledge the study of Xu et al.¹⁵ is the only phosphoproteomic analysis reported for PAH related cells and it focused on mitochondrial/metabolic perturbations. Kinases play a critical role in cell growth and proliferation, and there is a growing interest in the use of kinase inhibitors to address this underlying pathology.^{20–37} To understand the role of kinase signaling in PAH we performed an unbiased phosphoproteomic analysis of intact lung tissue from subjects with idiopathic PAH (iPAH) compared to control lung tissue.

Materials and methods

Phosphopeptide enrichment and mass spectrometry analyses

Tissue samples were obtained from the Pulmonary Hypertension Breakthrough Initiative (PHBI) tissue

repository.³⁸ Samples from iPAH were obtained at the time of lung transplantation. Control samples were obtained from donor lungs that were not used for transplant and were confirmed as being normal lungs free of pathology. The phosphoproteomic analysis was performed with frozen lung tissue from three iPAH female patients, three male iPAH patients, three female controls, and three male controls. Whole lung homogenates for each group were pooled, enriched for phosphoproteins by SCX/TiO₂, and then subjected to LC MS/MS. Label free quantitation was used to determine the relative differences in phosphopeptides between iPAH and controls.³⁹ Kinase predictions were made with NetworKin and PhosphoNet.^{40,41} Predictions were tested with in vitro phosphorylation assays. Gene ontology, reactome, and STRING network analyses were performed to identify candidate regulatory networks, and identify function and pathway enrichment.

Patient characteristics are shown in Table 1. PHBI patients' lung lysates samples were utilized for label free quantification. A sample preparation protocol was followed according to the method of Goel et al.⁴² to extract/precipitate, reduce and alkylate, and digest the proteins. Phosphopeptides from the digested proteins solution were then enriched by using titanium dioxide TopTips (GlySCi, Columbia, MD). The enriched phosphopeptides (bound) and flow through (non-bound) peptide fractions were collected using manufacturer's protocol and analyzed by LC-MS/MS using an Orbitrap Elite LC-MS/MS mass spectrometer equipped with a Waters nanoACQUITY Ultra Performance Liquid Chromatography (UPLC) and a Waters Symmetry[®] C18 180 μm × 20 mm trap column and a 1.7-μm, 75 μm × 250 mm nanoACQUITY UPLC column (35°C).

The collected LC-MS/MS data were processed with Progenesis QI Proteomics software (Nonlinear Dynamics, version 2.4) with protein identification carried out using

Table 1. Clinical characteristics of subjects from whom lung samples were obtained for phosphoproteomic analysis.

Clinical data				RHC data				Medications			
Subject	Diagnosis	Age	Sex	RA (mm Hg)	Mean PA (mm Hg)	PCWP (mm Hg)	CO (L/min)	Phosphodiesterase-5 (PDE-V) inhibitor	Endothelin receptor antagonist	Prostanoid	
1	iPAH	40	F	7	47	7	6.17		Ambrisentan	IV epoprostenol	
2	iPAH	41	F	30	55	7	3.86	Sildenafil	Bosentan	IV epoprostenol	
3	iPAH	38	F	NA	50	8	2.87	Sildenafil	Bosentan	IV treprostinil	
4	iPAH	25	M	NA	59	7	4.09	Sildenafil		IV epoprostenol/ SC treprostinil	
5	iPAH	40	M	NA	64	12	3.1	Sildenafil	Ambrisentan	SC treprostinil	
6	iPAH	51	M	NA	50	8	4.6	Sildenafil		IV epoprostenol	
10	Control	56	F								
11	Control	49	F								
12	Control	55	F								
13	Control	47	M								
14	Control	52	M								
15	Control	17	M								

the Mascot search algorithm. The Progenesis QI software performs chromatographic/spectral alignment (one run is chosen as a reference for alignment), feature/peptide extraction, data filtering, and quantitation of peptides and proteins. A normalization factor for each run was calculated to account for differences in sample load between injections as well as differences in ionization. The normalization factor was determined by comparing the total ion abundance among all the samples, with the expectation that they all should be the same based on the equal total amount of peptides that were loaded onto the column. The experimental design was setup to group multiple injections from each run. The algorithm then calculates the tabulated raw and normalized abundances, maximum fold change, and ANOVA *p* values for each feature in the data set. The MS/MS spectra were exported as “.mgf” (Mascot generic files) for database searching. The Mascot search results were exported as an “.xml” file using a significance cutoff of *p* < 0.05 and false discovery rate (FDR) of 1% and then imported into the Progenesis QI software, where search hits were assigned to corresponding peak features that were extracted from the MS data. Relative protein-level fold changes were calculated from the sum of all unique, normalized peptide ion abundances for each protein on each run. Only proteins with two or more unique quantifiable peptides were utilized in downstream analyses.

Kinase prediction

NetworKin was used to predict kinases that could phosphorylate the identified phosphopeptides. For a subset of phosphopeptides, the Kinexus prediction algorithm was used.⁴³ Prediction testing was performed for selected candidates with a phosphopeptide LC/MS/MS method and also with Kinexus in vitro radiometric assays.

Kinexus analysis

PhosphoNet was used to predict kinases that could phosphorylate a subset of phosphopeptides that were not amenable to prediction by NetworKin. A radiometric kinase assay was used to identify candidate kinases that phosphorylate IKZF3 and BCAS3 at the designated phosphorylation sites.

The following peptides were synthesized to screen IKZF3 and BCAS3:

Site	Name	Peptide sequence
IKZF3 [S378]	Wildtype (WT)	RERGLSPNN-pS-GHD
BCAS3 [S709]	Wildtype (WT)	RRHG-pS-YDSLASDH-pS-G
BCAS3 [A709]	Mutant (MT)	RRHG-pS-YD A LASDH-pS-G

For IKZF3, S382 was blocked by an attached phosphate group, so that 33P-label would not result on that site. In this way, the kinase screen was made specific for S378. The

kinases used in the in vitro assays were chosen based on predictions of PhosphoNet.

In vitro kinase assays with mass spectroscopic analysis

Substrate or control peptides were incubated in kinase assay and the applicable kinase for 60 min at 30°C. The reaction was terminated with EDTA and the samples stored at –80°C until analyzed. LC MS/MS analysis was performed using an Agilent 1100 series HPLC system coupled to an AB Sciex API 3000 Q-TRAP mass spectrometer with an HSI ionics upgrade. Ionization: electrospray ionization (ESI); polarity: positive; source voltage: 4800 V; temperature: 375°C; curtain gas: 12 AU; nebulizer gas (GS1): 12 AU; heater gas (GS2): 70 lbf/in². Scan conditions: scan range: 50.000 to 2200.000 amu; time: 1 s; declustering potential: 5 V; focusing potential: 5 V; entrance potential: 9 V; focusing lens (IQ1): –9.5 V; prefilter (ST): –9.5 V. HPLC conditions: injection volume: 10 µL; autosampler tray temperature: 4°C; flow rate: 0.3 mL/min; column: 4.6 × 100 mm Phenomenex Kinetic RP C18 (2.6 µM, 100 Å) with guard column and in-line filter; column oven: 20°C; mobile phase: A—0.1% formic acid in water, B—0.1% formic acid in acetonitrile; gradient: 0–4 min, 5%B; 4–14 min, 35%B; 14–15 min, 35%B; 15–15.5 min, 5%B; 15.5–20 min, 5%B.

Western blots and immunohistochemistry

A rabbit polyclonal IgG antibody was made against the N terminus of IKZF3 and a phospho specific site of Aiolos IKZF3 at the C-terminus (Thermo-Fisher, Waltham, MA). The antibodies underwent affinity purification and negative adsorption (Thermo-Fisher). The phospho-specific and total antibodies against Aiolos IKZF3 were used in Western blots to compare protein levels in iPAH, and controls.

Immunohistochemistry on formalin fixed paraffin embedded (FFPE) lung sections was performed with phosphorylated IKZF3 S378, total IKZF3, CD3 and CD20 antibodies. The phospho IKZF3 antibody was custom made. Western blot analysis was performed to measure the levels of pIKZF3 S378 and total IKZF3. A total of 50 µg of denatured protein was separated on SDS-PAGE and then transferred to nitrocellulose membrane. Nonspecific binding sites on the membrane were blocked by using TBS Starting Block (Cat# 37579, Thermo Fisher Scientific, Waltham, MA) for 1 h. at room temperature. The membranes were incubated overnight at 4°C with pIKZF3 S378 (Thermo Scientific, Waltham, MA) and total IKZF3 antibodies (Thermo Scientific). After three washes in TBST, the membranes were incubated with anti-rabbit horseradish peroxidase-coupled secondary antibody (Cell Signaling Technologies, Danvers, MA) for 1 h at room temperature. After washing the membranes thrice in TBST, the immunoreactive proteins were visualized by adding Super Signal West Femto

Substrate (Thermo Scientific). The images were developed on c-DIGIT Blot-Scanner (LICOR, Lincoln, NB) per the manufacturer's instructions. The immunoreactive bands were quantified by densitometry.

RNA*Scope* assay

Human lung samples were obtained from the PHBI tissue repository. In situ hybridization (ISH) with a probe specific for IKZF3 (NM_012481.5) was performed with an RNA*Scope* Assay (Advanced Cell Diagnostics, Newark, CA.) on 20 FFPE human lung tissue samples. Five control samples from potential donors not used for lung transplant, 10 iPAH samples, and 5 associated with PAH (APAH) samples obtained at the time of lung transplant were studied. A pathologist (at ACD) evaluated the IKZF3 expression in two ways. The first used a semi-quantitative scoring system to evaluate the number of IKZF3 "dots" per cell where each dot signifies detection of one gene transcript. A score of 0 represents <1 dot/cell, a score of 1 represents 1–3 dots/cell, a score of 2 represents 4–9 dots per cell, a score of 3 represents 10–15 dots/cell and a score of 4 represents >15 dots per cell. The second method estimated the percent of cells expressing IKZF3. The two methods were applied globally to an entire scanned section for each sample, and percent expression was used to evaluate cells in lymphoid clusters or aggregates where they occurred in each sample.

Lentivirus transduction

All lentivirus particles were purchased from GeneCopoeia (Rockville, MA). Lentivirus particles for wildtype IKZF3 (WT-IKZF3), mutant IKZF3 S378A (IKZF3 S378A), and three point mutant IKZF3 S378A;S386A;S391A (IKZF3 tri) had the *neo* gene (neomycin resistant gene). Lentivirus particles for BCL2 promoter-*luciferase* reporter had the *pac* gene (puromycin resistance gene). Both IKZF3 and the BCL2 promoter reporter were expressed in MRC5 cells and HEK 293 cells using lentivirus transduction. Briefly, cells were plated on six-well plates at a concentration of 2.5×10^4 cells/well and allowed to adhere to the plate overnight. Lentivirus particles were added to the cell culture media of the cells. A positive selection of stable transduced cells were performed after three days using G418 (Geneticin) or Puromycin for IKZF3 and its mutants, and BCL2 promoter-*luciferase* reporter, respectively. These cells were used for measuring BCL2 promoter-*luciferase* reporter activity.

BCL2 promoter-*luciferase* reporter assay

The Secrete-Pair™ Dual Luminescence Assay Kit (GeneCopoeia) was used to measure BCL2 promoter reporter–Gaussia luciferase (Gluc) and secreted alkaline phosphatase activities as per the manufacturer's protocol.

Statistical and pathway analyses

ANOVA followed by the Bonferroni correction, the Kruskal–Wallis test followed by the Steel–Dwass–Critchlow–Fligner procedure, or Dunn's test with the Bonferroni correction were used to evaluate differences between groups. IKZF3 Western blot quantification was analyzed using Student's *t*-test. Unless otherwise indicated data are presented as mean \pm SEM. Statistical significance was set at $p < 0.05$.

Pathway analyses were performed with STRING (<https://string-db.org>), Gene Ontology Tools (Lewis Sigler Institute, go.princeton.edu), and Reactome (reactome.org).

Results

iPAH analysis

There were 60,428 features generated in the enriched phosphopeptide analysis. From these features 6622 proteins were identified. Within the subset of identified proteins there were 1479 phosphopeptides with $q < 0.05$. With removal of redundancies this number was reduced to 1234. The relative enrichment of phosphopeptides with $q < 0.05$ in female iPAH vs. female controls, and male iPAH vs. male controls was determined. Fig. 1 depicts a volcano plot of log₂ enrichment vs. $-\log p$ value for the phosphopeptides in the female iPAH group vs. controls. The 10 most increased and 10 most decreased phosphopeptides are shown in Tables 2 and 3 for females and males. The full list is shown in the Full List Phosphopeptide Excel file Supplement. The most dramatic finding was a high and categorical abundance of the phosphopeptide IKZF3 phosphorylated at S378 in both female and male iPAH, with no detection in control samples. High relative abundance in iPAH females without detection in female controls was also found for a phosphopeptide corresponding to S73 of HMHA-1 (minor histocompatibility factor 1). This phosphopeptide was increased over six-fold in male iPAH relative to male controls.

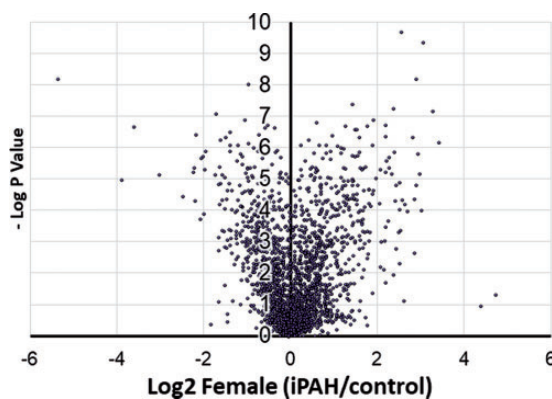


Fig. 1. Volcano plot of phosphopeptides for female iPAH/control subjects generated from phosphoproteomic analysis.

Table 2. The 10 most increased phosphopeptides found in the phosphoproteomic analysis from females and males.

Protein	Sequence	Variable modifications ([position] description)	Description	Ratio female iPAH/female control	Ratio male iPAH/male control
IKZF3	GLSPNNSGHDSTDTDSNHEER	[3] Phospho (ST)	Zinc finger protein Aiolos	#DIV/0!	#DIV/0!
HMHA1	HASAAGFPLSGAASWTLGR	[3] Phospho (ST)	Minor histocompatibility protein HA-1	#DIV/0!	6.49
BCAS3	HGSYDSLASDHSGQEDEE	[6] Phospho (ST)	Breast carcinoma-amplified sequence 3	119.26	10.70
RHG25	WLSQVEIVTHTGPHR RTQTLPNRK	[4] Phospho (ST)	Rho GTPase-activating protein 25	18.95	2.75
NUMA1	RQSMAFSILNTPK	[3] Phospho (ST)	Nuclear mitotic apparatus pro- tein 1	15.32	#DIV/0!
LEUK	RPTLTTFGR	[3] Phospho (ST)	Leukosialin	11.94	2.26
MUC1	DTYHPMSEYPTYHTHGR	[11] Phospho (ST)	Mucin-1	10.64	14.23
NU214	TPSIQPSLLPHAAPFAK	[3] Phospho (ST)	Nuclear pore complex protein Nup214	10.40	4.09
WDR24	IYCSPLVPTANLNHNSVGK	[4] Carbamidomethyl (C) [11] Phospho (ST)	WD repeat-containing protein 24	10.27	3.35
NUMA1	RASMQPIQIAEGTGITTR	[3] Phospho (ST)	Nuclear mitotic apparatus pro- tein 1	9.73	12.12

The phosphopeptide corresponding to S709 of BCAS3 (Breast Cancer Amplified Sequence 3) was increased 119-fold in female iPAH and 10-fold in male iPAH relative to their respective controls. Phosphopeptides with low relative abundance in iPAH females and males relative to controls included phosphorylated forms of HDAC2, brain specific angiogenesis inhibitor 1 associated protein 2-like protein (BI2L2), S100-A9, Annexin A2, PC4 and SFRS1-interacting protein (PSIP1), HIV Tat-specific factor 1 (HTATSF1), putative synaptogyrin-2 like protein (SNG2L), and receptor-type tyrosine-protein phosphatase beta (PTPRB).

The NetworKin analysis was performed on the enriched phosphopeptides to predict what kinases might be responsible for their phosphorylation. The full output consisted of 9684 predictions. NetworKin prediction scores can range from 1 to 60. A score of 60 indicates high probability of a correct prediction, a score of 1 indicates low probability. The subset of predictions with NetworKin scores over 9 consisted of 207 predictions.

Supplement Table 1 shows the list of the most frequent kinases predicted by NetworKin with scores >9. The most frequent kinases were CSNK2A1 (casein kinase 2), and cyclin-dependent kinase 1 (CDK1), followed by MAP kinases and PRKs. Less frequent kinases included AKT1, Aurka, CamK2B, GSK3A, GSK3B, HPK2, HYRC, and PAKs 2,3, and 4. PDK1 (3-phosphoinositide-dependent protein kinase Accession NP_002604.1) was predicted to phosphorylate mechanistic target of rapamycin kinase (MTOR) at S2481 and S1261 with high scores. Predictions for PAK3 (with substrate from NCK1), Aurka (substrate from NUMA1), CDK1 (substrate from NCOR), and CSNK2A1 (substrate from HDAC2) were confirmed by in

vitro phosphorylation assays. PAK1 did not phosphorylate the peptide sequence from BCAS3 (the NetworKin Prediction score for this peptide was low). A limitation of NetworKin was that it did not provide kinase predictions for some of the most up-regulated or down-regulated 10 phosphopeptides.

Gene ontology analyses. Gene ontology analysis was performed using the phosphopeptide list (Supplement) and search terms for immune regulation, angiogenesis and cell proliferation as well as an agnostic search. The 1234 phosphopeptides mapped to 761 genes (473 “duplications” due to different phosphorylation sites on the same protein). Of the 761 genes, 61 were not annotated. Therefore the analysis was done on 700 genes. One hundred seventy-two genes mapped to immune system regulation (24.57%; GO:0002376). One hundred five mapped to cell proliferation (15%, GO:0008283) and thirty-five mapped to angiogenesis (5.00%, GO:0001525; Supplement Table 2). The PANTHER GO-Slim Molecular function analysis revealed enrichment in RHO GTPase related molecules among others (Supplement Table 3).

Reactome analysis. The reactome analysis revealed significant enrichment for proteins involved in the RHO GTPase cycle, RAC1 GTPase cycle, neutrophil degranulation, signaling by v-raf murine sarcoma viral oncogene homolog B1 (BRAF) and rapidly accelerated fibrosarcoma (RAF) fusions, MAP2k and mitogen-associated protein kinase (MAPK) activation, oncogenic MAPK signaling, and glycolysis (Supplement Table 4).

Table 3. The 10 most decreased phosphopeptides from the phosphoproteomic analysis of females and males.

Protein	Sequence	Variable modifications ([position] description)	Description	Ratio female iPAH/control	Ratio male iPAH/control
PKP3	TLQRLSSGFDDIDLPSAVK	[6] Phospho (ST) [7] Phospho (ST)	Plakophilin-3	0.2281	1.0561
FRIH	MGAPESGLAEYLFDKHTLGDSDNES	[25] Phospho (ST)	Ferritin heavy chain (Ferritin H subunit) (EC 1.16.3.1)	0.222	0.4834
BI2L2	LMSSEQYPPQELFPR	[3] Phospho (ST)	Brain-specific angiogenesis inhibitor 1-associated protein 2-like protein 2	0.2094	1.3587
PLD1	MSLKNEPRVNTSALQK	[11] Phospho (ST) [12] Phospho (ST)	Phospholipase D1 (PLD 1) (hPLD1) (EC 3.1.4.4)	0.1781	0.8217
SRSF2	SRSPPVSK	[3] Phospho (ST)	Serine/arginine-rich splicing factor 2 (Protein PR264)	0.1286	0.2777
ANXA2	IMVSRSEVDMLKIR	[4] Phospho (ST) [10] Oxidation (M)	Annexin A2 (Annexin II) (Annexin-2)	0.0244	0.0768
PSIP1	TGVTSTSDSEEGDDQEGEK	[9] Phospho (ST)	PC4 and SFRS1-interacting protein (CLL-associated antigen KW-7)	0.0199	0.0433
HTSF1	VLDEEGSEREFDEDSDEKEEEDTYEK	[15] Phospho (ST)	HIV Tat-specific factor 1 (HTAT-SF1)	0.0186	0.2812
SNG2L	ALCLVFALIVFSCIYGEGYSNTHKSK	[3] Carbamidomethyl (C) [13] Carbamidomethyl (C) [19] Phospho (Y) [20] Phospho (ST) [22] Phospho (ST) [25] Phospho (ST)	Putative synaptogyrin-2 like protein	0.0074	0.2726
PTPRB	FGVSKEK	[4] Phospho (ST)	Receptor-type tyrosine-protein phosphatase beta (protein-tyrosine phosphatase beta) (R-PTP-beta) (EC 3.1.3.48) (vascular endothelial protein tyrosine phosphatase) (VE-PTP)	0	0

STRING database network analysis

A STRING database network analysis was performed for the following: (1) CSNK2A1, CSNK2A2, CDK1 (Supplement Figure 1); (2) Rho-GTPase and related proteins (Supplement Figure 2); (3) MAP kinases (Supplement Figure 3); (4) PRK kinases with NetworKin score >9 (Supplement Figure 4); (5) PRKG kinases (Supplement Figure 5); (6) AKT (Supplement Figure 6); (7) Aurka (Supplement Figure 7); (8) CAMK (Supplement Figure 8); (9) GSK3A and GSK3B (Supplement Figure 9); (10) HPK2 and HYRC (PRKCD; Supplement Figure 10); (11) PAK1,2,3, and 4 (Supplement Figure 11). Although the NetworKin prediction scores for PRKG were relatively low, the STRING analysis showed significant interconnectivity of the kinase with the corresponding phosphoproteins.

Key targets for CSNK2A1 and CSNK2A2 are shown in Supplement Table 5, with relative abundance of the corresponding phosphopeptides in iPAH female and males relative to controls. Interestingly, a recent whole blood RNA sequencing effort in PAH suggested differential regulation of CSNK2A1 at the level of gene expression in circulating cells.¹¹ The targets of CSNK2A1 and CSNK2A2 included HAP28 (PDGFA associated protein 1), DVL3, HNRNPC, HDAC2, IGF2R, and CCNH. The corresponding 12 phosphopeptides for HDAC2 were significantly decreased in iPAH females and males relative to controls. The regulation of HDAC2 in iPAH is relevant due to recent interest in targeting histone deacetylases as a treatment for PAH.⁴⁴⁻⁴⁷

Key targets for CDK1 are shown in Supplement Table 6, and include, NUMA1, NCOR, KAT7, NUCKS, LMNA, EEF1d, and TP53B. The phosphopeptides from NUMA1

and NCOR were significantly increased in iPAH females and males relative to controls. The NUCKS phosphopeptide was significantly decreased in iPAH females and males relative to controls.

3-Phosphoinositide-dependent protein kinase (PDK1) was predicted to phosphorylate MTOR at S2481 with a score of 60, and at S1261 with a score of 25.6. AMPKa2 (PRKAA2) was also predicted to phosphorylate MTOR at S1261 with a NetworKin score of 16. Phosphorylation at this site was 3.2- and 3.3-fold increased in iPAH females and males relative to their respective controls. Phosphorylation at S2481 was increased 3.8-fold in female iPAH but was not regulated in male iPAH. MTOR was also a focal point of the PRK network.

Kinexus assays

Radiometric assays were performed to identify candidate kinases that could phosphorylate sequences for the following sites: S378 IKZF3, and S709 BCAS3. The results are shown in Supplement Tables 7 and 8.

In vitro kinase assays with mass spectroscopic analysis

Supplement Table 9 shows the results of the in vitro kinase assays with HPLC MS/MS analysis.

Western blots and immunohistochemistry

Western blots demonstrated an increase in S378 phosphorylated IKZF3 (Aiolos; pIKZF3) in iPAH lung extracts compared to controls (Fig. 2(a)). Immunohistochemistry localized pIKZF3 to perivascular infiltrates and neointimal lesions of pulmonary arterioles in iPAH (Figs. 2(b) and 3). The perivascular infiltrates consisted of a mixed population of CD3+, CD8+Tcells, and CD20+ B cells. CD45ra+ T

cells were also detected but to a lesser degree (Fig. 4). Immunohistochemistry with an anti-HMHA1 antibody also confirmed the presence of HMHA1 in perivascular infiltrates in PAH samples (Fig. 4).

RNAScope

The clinical characteristics of the subjects from whom lung samples were obtained for the RNAScope assay are shown in Supplement Table 10. The results of the semi-quantitative analysis are shown in Supplement Table 11. ISH demonstrated the presence of IKZF3 mRNA primarily in lymphoid aggregates adjacent to remodeled pulmonary arteries, or bronchioles. The IKZF3 signals were concentrated in these regions of inflammatory cells and were increased in most iPAH samples compared to controls in these regions (Fig. 5). The global scores were 1 for all the controls, all the APAH evaluable samples, and 6 of the iPAH samples. The scores were 1–2 for two iPAH samples, and 0 for two iPAH samples. Percent of lymphoid cells expressing IKZF3 was 1–10% for one control, 11–25% for four controls, 11–25% for one APAH sample, 26–50% for three APAH samples, 1–10% for four iPAH samples, 11–25% for three iPAH samples, and 51–75% for three iPAH samples. QC failed one APAH sample.

BCL2 luciferase reporter assay

IKZF3 has been reported to function as a transcription factor for BCL2. Therefore, we performed a series of experiments to explore the potential role of phosphorylation on the function of IKZF3 in a BCL2 luciferase reporter assay. Co-transduction experiments were performed to examine the effect of changing 1–3 serine phosphorylation sites of IKZF3 on BCL2 promoter activity. Fig. 6(a) demonstrates

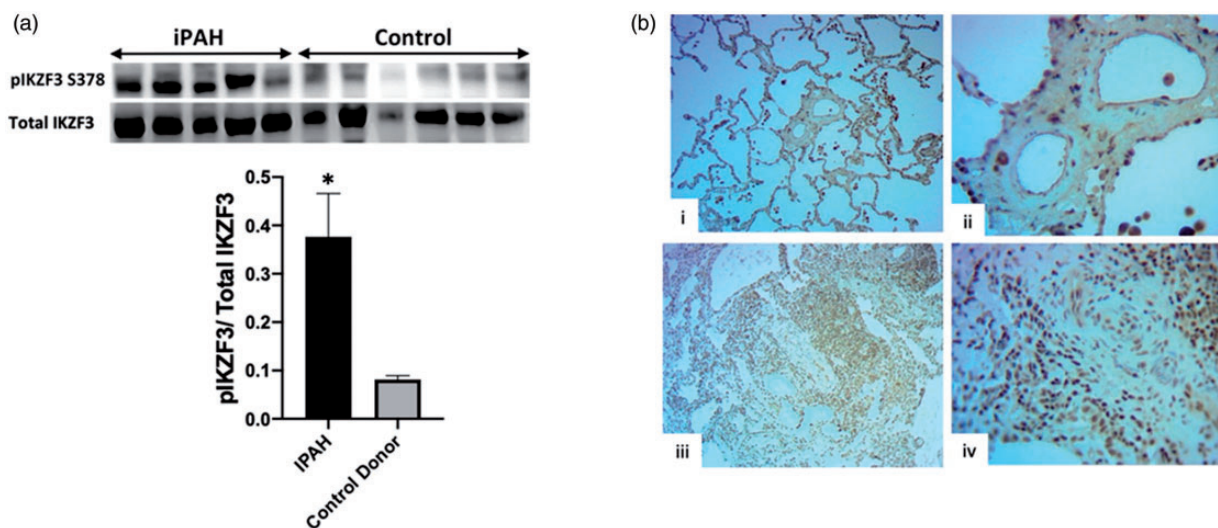


Fig. 2. (a) Western blots with phospho-specific and total IKZF3 antibodies in lung tissue lysates. Control ($n = 6$) and iPAH ($n = 5$). $*p < 0.05$ vs. control. (b) Immunohistochemistry with pIKZF3 antibody: comparison of control (i and ii) to iPAH (iii and iv). Cells staining positive for phosphorylated S378 IKZF3 congregate densely around a hypertrophied pulmonary arteriole.

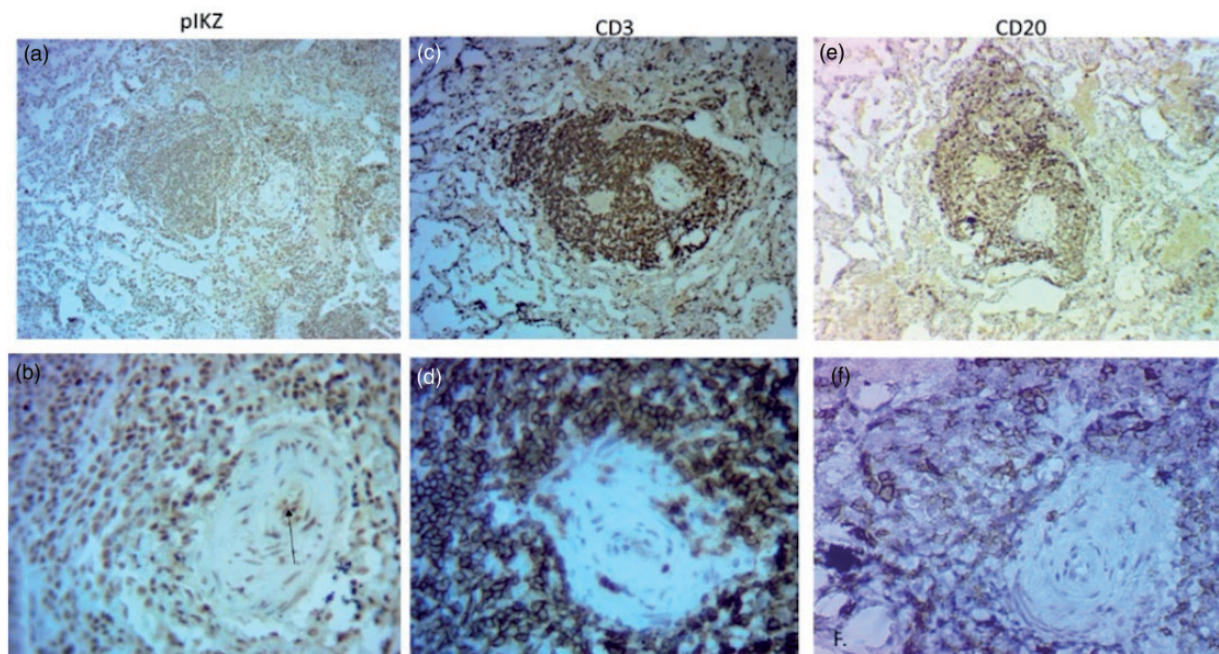


Fig. 3. Immunohistochemistry of iPAH lung tissue, showing inflammatory perivascular infiltrates. CD3: antibody against a T-cell marker; CD20, antibody against B-cell marker. pIKZF3, antibody against S378 phosphorylated Aiolos. pIKZ was present predominantly in perivascular cells, but was also seen in endothelial-like cells of the diseased pulmonary arteriole (arrow). (a) pIKZ 10 \times objective. (b) pIKZ 40 \times objective (arrow points to small lumen of pulmonary arteriole with staining of endothelium). (c) CD3 T cell marker 10 \times objective. (d) CD3 T cell marker 40 \times objective. The T cells were primarily perivascular. There were more T cells than B cells. (e) CD20, B cell marker 10 \times ; (f) CD20 B cell marker 40 \times objective.

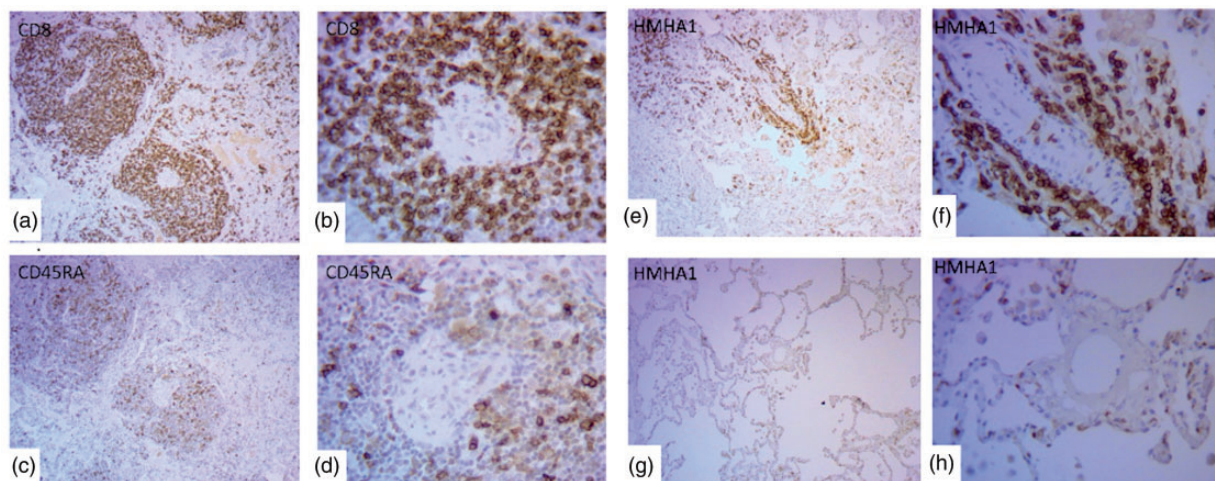


Fig. 4. The perivascular infiltrates seen in iPAH lung sections were highly positive for CD8 ((a) 10 \times objective, (b) 40 \times). Scattered cells in the perivascular infiltrates stained positive for CD45RA ((c) and (d)). CD45RA is a protein tyrosine phosphatase and is believed to be a marker for cytolytic T lymphocytes. HMHA1 in perivascular infiltrates in APAH SSC lung sample ((e) 10 \times , (f) 40 \times objective) vs. control sample ((g) 10 \times , (h) 40 \times objective). Cells surrounding a pulmonary arteriole were highly positive for HMHA-1 in a PAH lung sample.

by Western blot an example of a lentiviral transduction of wild type IKZF3 into MRC5 cells. Wild type IKZF3 and IKZF3(S378A) both increased BCL2 reporter activity, whereas IKZF3 (S378A, S386A, and S391A) did not increase BCL2 reporter activity over baseline (Fig. 6(b)).

Discussion

In this study we performed an unbiased phosphoproteomic analysis of lung tissue from iPAH subjects. While several proteomic analyses have been reported related to PAH, to our knowledge this is the first phosphoproteomic analysis of

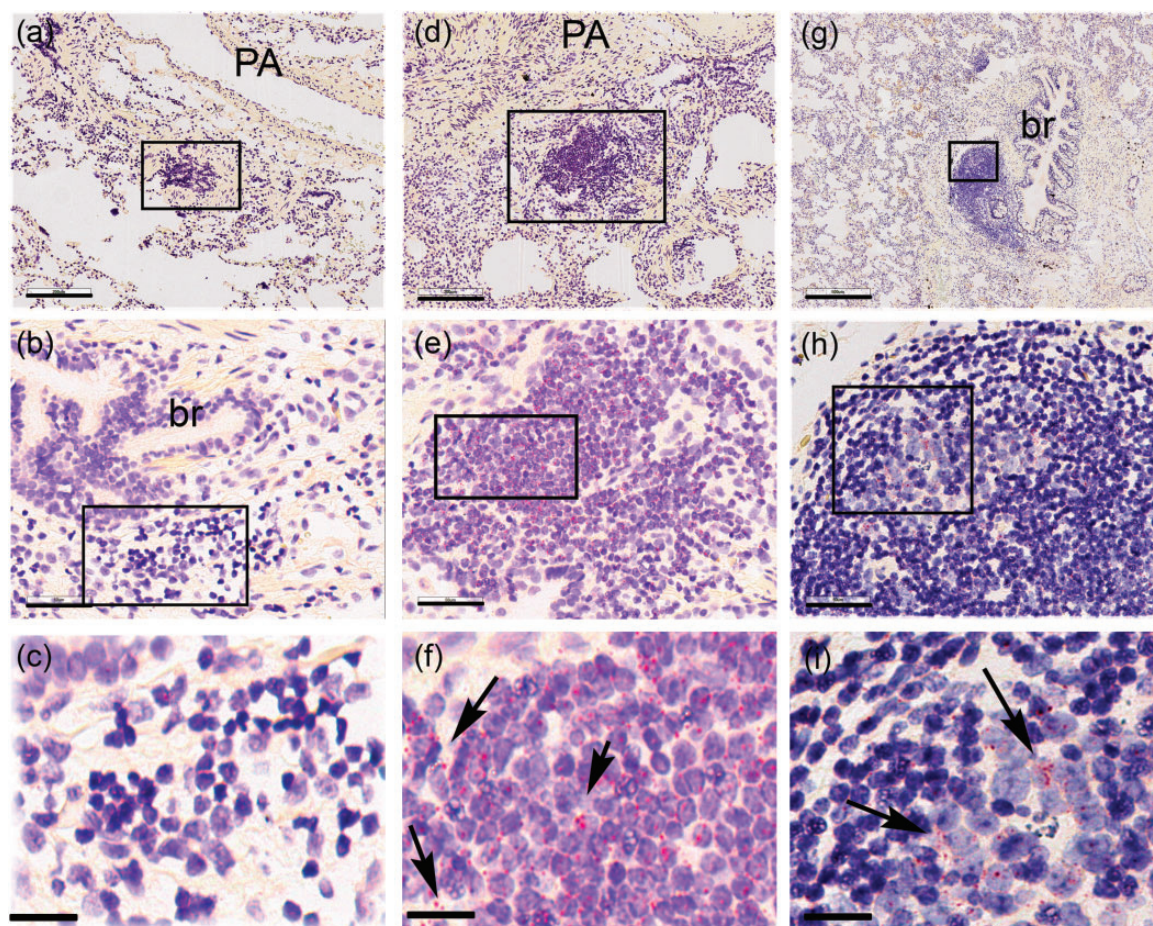


Fig. 5. In situ hybridization for IKZF3 in control ((a) to (c)), IPAH ((d) to (f)), and APAH ((e) to (g)) representative lungs. IKZF3 mRNA expression was minimal or absent in control lungs, while consistently expressed in lymphoid aggregates adjacent to remodeled pulmonary arteries (PA) and terminal bronchioles (br) in IPAH and APAH (arrows). The highlight boxed areas in (a), (d), and (g) are magnified in (b), (e), and (h), respectively. Boxed regions in (b), (e), and (h) are further magnified in (c), (f), and (i), respectively (magnification bar (a), (d), (g): 200 μ m; (b), (e), (h): 50 μ m; (c), (f), (i): 12.5 μ m).

intact iPAH lung tissue.^{10,15,48–52} We compared the relative abundance of phosphopeptides in iPAH females to female controls, and iPAH males to male controls. Several novel phosphopeptides were at substantially higher levels in iPAH samples compared to controls. The most dramatically increased phosphopeptide was from a zinc finger transcription factor IKZF3, followed by a phosphopeptide from HMHA1. The third most increased phosphopeptide was from BCAS3 which was increased in both male and female iPAH samples. We also found several phosphopeptides that were markedly decreased in iPAH samples relative to controls. These included S100-A9, Annexin A2, PC4 and PSIP1, HTATSF1, SNG2L, and PTPRB.

NetworKin was used to predict what kinases could phosphorylate the differentially regulated phosphopeptides identified in the primary phosphoproteomic analysis. The NetworKin analysis was successful in generating high probability prediction scores for a number of kinases, though many of the most highly regulated phosphopeptides did not yield kinase predictions. In select cases we confirmed

the NetworKin predictions with in vitro kinase assays. For the phosphopeptides corresponding to IKZF3, HMHA1, and BCAS3, we used PhosphoNet to predict which kinases might be responsible for the phosphorylation of the identified phosphopeptides. These predictions were tested for IKZF3 and BCAS3 with custom designed Kinexus assays. Based on the finding that pIKZF3 was markedly increased in iPAH lungs relative to control lungs (where no signal for pIKZF3 was detected), we focused our attention on this protein for further study using traditional biochemical techniques. To place our results in the context of known signaling pathways additional bioinformatic analyses were performed. These analyses included Gene Ontology, Reactome, and STRING, and demonstrated the potential importance of other key pathways implicated in PAH such as RHO-GTPase signaling, protein kinase CGMP-dependent 1 (PKG1)- and PTPRB-mediated signaling. More detailed discussions of other highly regulated targets and the results of the NetworKin analysis are found in the Supplement.

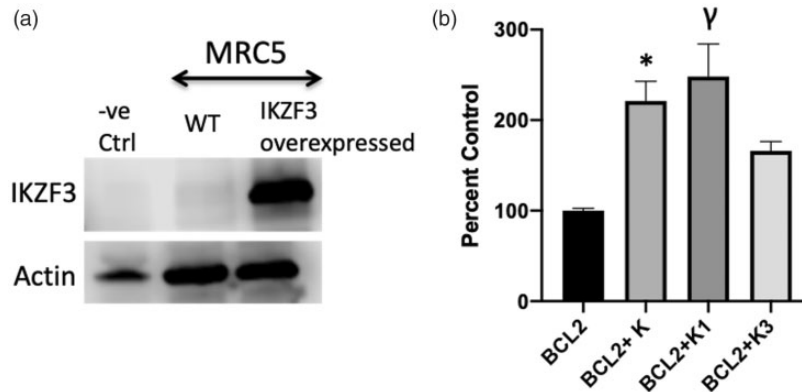


Fig. 6. (a) IKZF3 overexpressed using lentivirus transduction. The Western blot image shows an example of lentivirus transduction of IKZF3 in MRC5 cells. (b) Effect of wild type IKZF3 (K), IKZF3 (S378A) (K1), or IKZF3 (S378A, S386A, and S391A) on BCL2 reporter activity expressed as percent control (BCL2 = control). Lentivirus-induced WT IKZF3 expression in cells increased BCL2 promoter reporter activity measured by luciferase assay. Wild type and IKZF3 (S378A) increased BCL2 reporter activity, additional mutations of serine phosphorylation sites reduced the response to IKZF3 co-expression suggesting a phosphorylation dose effect ($*p = 0.003$, $\gamma p = 0.0013$ vs. BCL2 control).

After mapping the phosphoproteins to their respective genes, the gene ontology analysis revealed several genes involved in immune regulation, cell proliferation, and angiogenesis. The reactome analysis found significant over-representation of proteins involved in RHO and RAC1 GTPase cycles, as well as signaling by BRAF and RAF fusions, MAPK and glycolysis. STRING analyses also identified high interconnectivity in RHO GTPase proteins, and interconnectivity of the MAPK pathways that emerged from the phosphoproteomic results.

The potential importance of RHO-GTPase cycling in PAH is highlighted by the increased phosphorylation of HMHA1 found in the phosphoproteomic analysis because HMHA1 was recently identified as a Rho-GTPase.⁵³ A BAR domain at the N-terminal region of the HMHA1 was found to autoinhibit the Rho-GAP domain. This auto-inhibition was demonstrated through deletion of the BAR domain which allowed emergence of the Rho-GTPase functionality. It is possible that phosphorylation of one or more regions of HMHA1 could alter its Rho-GTPase activity by preventing autoinhibition by the BAR domain.⁵³ Rho-GTPases are known to affect actin organization, cell shape, and cell spreading. HMHA-1 was shown to colocalize with the Rho-GTPase Rac1.⁵⁴ BMPR2 mutations seen in PAH may result in activation of RAC1 and thereby alter organization of the cytoskeleton. Expression of HMHA1 was previously thought to be restricted to hematopoietic cells and epithelial tumor cell lines. However, a recent gene expression study in Zebrafish suggests that HMHA1 along with Rasip1 may be expressed in endothelial cells.⁵⁵ Immunohistochemistry in the PAH samples we examined showed localization of HMHA1 to perivascular infiltrates.

In female and male iPAH samples, phosphorylation of PTPRB (P23467), a protein tyrosine phosphatase (PTP), was not detected at S119. In pulmonary artery smooth muscle cells (PASMCs) hypoxia decreased expression of

several PTPs (T cell PTP, density-enhanced phosphatase-1, PTP1B, and SH2 domain-containing phosphatase-2), resulting in reduced PTP activity. Hypoxia-inducible factor HIF-1alpha was involved in this regulation of gene expression because HIF-1 alpha siRNA abolished hypoxia-induced PDGFR beta hyperphosphorylation and PTP down-regulation. PDGFR beta hyperphosphorylation and PTP down-regulation were also present in vivo in mice with chronic hypoxia-induced pulmonary hypertension.⁵⁶ While the effect of decreased S119 PTPRB phosphorylation is not known, loss of function mutations in PTPRB have been associated with angiosarcomas.⁵⁷ We hypothesize that decreased PTPRB phosphorylation could decrease PTPRB activity and thereby increase the phosphorylation state and activation of the PDGF beta receptor. These effects in turn could lead to pulmonary arteriolar myofibroblast and smooth cell proliferation, a hallmark of the abnormal pulmonary arteriole remodeling observed in PAH.

NetworkKin predicted PRKG1 as a kinase that could phosphorylate PTPRB at S119. Network analysis of PRKG1 candidate phosphorylation substrates from the phosphoproteomic analysis is shown in Supplement Figure 5. PRKG1 is a cyclic GMP-dependent kinase which is known to phosphorylate PPP1R12A, a phosphatase that increases the activity of myosin phosphatase regulatory targeting subunit 1 (MYPTL1). PRKG1 may also phosphorylate protein phosphatase 1, regulatory (inhibitor) subunit 14A (PPP1R14A); PPP1R14A is an inhibitor of PPP1CA and has over 1000-fold higher inhibitory activity when phosphorylated, creating a molecular switch for regulating the phosphorylation status of PPP1CA substrates and smooth muscle contraction. ROCK 1 and ROCK 2 phosphorylate myosin phosphatase target subunit 1 (MYPT1) at T696 and T853, the effect of which is to decrease MYPT1 phosphatase activity against myosin light chain kinase. This decreased dephosphorylation results in increased SMC contractility. In contrast PKG

phosphorylation of MYPT1 at S668, S692, S695, and S852 increase MYPT1 activity.⁵⁸ Degradation of MYPT1 led to the development of tolerance to nitric oxide in porcine pulmonary artery.⁵⁹ It was recently shown that BMP signaling via Smad1/5/8 required cyclic guanosine monophosphate (cGMP)-dependent protein kinase isotype I (PKG1) to maintain PSMCs in a differentiated, low proliferative state. BMP cooperation with cGMP/PKG1 was required for transcription of contractile genes and suppression of pro-proliferative and anti-apoptotic genes. Lungs from mice with low or absent PKGI (Prkg1(+/-) and Prkg1(-/-) mice) exhibited impaired BMP signaling, decreased contractile gene expression, and abnormal vascular remodeling. Conversely, cGMP stimulation of PKGI restored defective BMP signaling in rats with hypoxia-induced PAH, consistent with cGMP-elevating agents reversing vascular remodeling in this PAH model.⁶⁰ In our phosphoproteomic analysis, the phosphopeptides identified as substrate candidates for PKG were markedly decreased relative to controls. These data lead to the hypothesis that tolerance to drugs which act by increasing cGMP (i.e. PDE-V inhibitors) could result from down-regulation of PKG1. Strategies to increase PKG1-mediated signaling and PTPRB activity could provide a new approach to treating PAH.

The most up-regulated phosphopeptide in female and male iPAH vs. controls in the phosphoproteomic analysis was identified as a sequence from IKZF3 which encodes the zinc finger protein Aiolos (named after the Wind God of Greek mythology); these findings were confirmed by Western blot and immunohistochemistry. Phosphorylated IKZF3 was localized to perivascular infiltrates in iPAH lungs and the perivascular cells were predominantly T cells with some B cells which were minimal or absent in normal controls. ISH with an IKZF3 probe was used in an RNAscope assay to examine cell level gene expression of IKZF3 in iPAH and APAH lung samples obtained at the time of lung transplant compared to controls obtained from potential donors whose lungs were not used for transplant. IKZF3 expression was restricted for the most part to perivascular inflammatory cells and lymphoid aggregates consistent with the findings of immunohistochemistry. A semi-quantitative analysis showed heterogeneity of gene expression in iPAH and APAH samples, but an overall increase compared to control samples. The heterogeneity may reflect sampling bias, or could represent a spectrum of inflammatory signaling in these end-stage samples. It should also be kept in mind that the immunohistochemistry and Western blot analyses examined the phosphorylation state of the IKZF3 protein, Aiolos, which represents a level of regulation different than that of gene expression.

A Kinexus screen identified GSK2-alpha and GSK3-beta as kinases that phosphorylate S378 of IKZF3 (Aiolos). DYRK2 also phosphorylated S378 of IKZF3 but at lower levels than GSK3-alpha or GSK3-beta. Interestingly GSK3-

beta was shown to be increased in human PAH and animal models of PAH, and to mediate PDGFBB stimulated PASM C proliferation.⁶¹ These effects were found to involve cross talk between PDGFBB and Wnt/beta catenin signaling.⁶²

Aiolos (the protein product of IKZF3), Ikaros, Eos, and Helios are zinc finger transcription factors involved in lymphoid cell line differentiation.⁶³⁻⁷² Aiolos is highly expressed in several B and T cell lineages, and has been found to play a role in the pathogenesis of certain leukemias, lymphomas, and multiple myeloma.⁷³⁻⁷⁷ In some settings, Aiolos decreases apoptosis by suppressing PTEN (phosphatase and tensin homologue deleted on chromosome 10) and activating the phosphatidylinositol-3-kinase/Akt signaling pathway.⁷⁸⁻⁸⁰ Interestingly, in a recent report of RNA sequencing of whole blood as well as a lung transcriptomic study in PAH, PTEN was highly and significantly differentially regulated.^{11,17} In other settings, Aiolos and Ikaros can increase apoptosis and inhibit growth by suppressing c-Myc.⁸¹ IKZF3/Aiolos has also been shown to be involved with transforming growth factor beta 1 signaling and interacts with SMAD1 to induce Fox3 positive lymphoid Treg cells.⁸² Thus the functional effects of Aiolos appear to be context dependent.

Recent reports have found that IPAH lungs contained perivascular tertiary lymphoid tissues (tLTs), comprising B- and T-cell areas with high endothelial venules and dendritic cells. Lymphocyte survival factors, such as IL-7 and platelet-derived growth factor-A, were expressed in tLTs as well as the lymphorganogenic cytokines/chemokines, lymphotoxin-alpha/-beta, CCL19, CCL20, CCL21, and CXCL13.⁸³ In a study of circulating cells in PAH patients, significantly fewer CD8+ T cells but more CD25hi+ and FoxP3+CD4+ T cells were found in the peripheral blood of patients compared with controls.⁸⁴ In another series, IPAH patients were found to have abnormal circulating CD8+ T lymphocyte subsets, with a significant increase in CD45RA+ CCR7-peripheral cytotoxic effector-memory cells and reduction of CD45RA+ CCR7+ naive CD8+ cells versus controls. Furthermore, IPAH patients had a higher proportion of circulating regulatory T cells (T(reg)) and four-fold increases in the number of CD3+ and CD8+ cells in the peripheral lung compared with controls.⁸⁵ CD45RA is a PTP and is believed to be a marker for T lymphocytes with greater cytolytic activity and greater propensity to travel to non-lymphoid tissues.⁸⁵ Our findings of high density CD8+ and CD45A+ cells in perivascular infiltrates in iPAH confirm those of Austin et al.⁸⁵ and demonstrate the new finding of increased pIKZF3 in these infiltrates. Studies of immortalized B cells and circulating B cells have shown distinct RNA transcript profiles in PAH compared to controls suggesting an important role of B cells in PAH pathobiology.^{13,14}

Our results suggest that IKZF3/Aiolos may play a key pathogenetic role in PAH. Results from the BCL2 reporter

assay indicate that wild type IKZF3 increases BCL2 transcription. Changing the serine to alanine at position 378 did not markedly decrease BCL2 reporter activity but removing additional serines near S378 such as S386 and S391 did decrease BCL2 activity bringing it back towards control levels. Recently it has been shown that BCL2 is increased in PAH pulmonary arterial endothelial cells.⁸⁶ Furthermore, iPAH pulmonary artery smooth muscles cells have been shown to resist apoptosis and it has been proposed that this resistance may be due to an increase in the BCL2/Bax ratio.⁸⁷ BCL2 may play an important role in PAH because it has been shown that BMPR2 deficiency mediates effects via an isoform switch from a pro-apoptotic to an anti-apoptotic form of BCL.⁸⁸ The functional effects of Aiolos activation may play a role in this switch to an anti-apoptotic state in perivascular lymphocytes in iPAH, and deserve further study.

To our knowledge, this is the first reported phosphoproteomic analysis of intact iPAH lung samples. It revealed a dramatic increase in several previously unreported targets including phosphorylated IKZF3 (Aiolos), a zinc finger transcription factor involved in lymphocyte regulation, HMHA1 a Rho-GTPase, and BCAS3, a protein involved in regulating angiogenesis. Conversely, significantly decreased phosphorylation of HDAC2, S100-A9, Annexin A2, PC4 and PSIP1, HTATSF1, SNG2L, and PTPRB were found. A Reactome analysis demonstrated overrepresentation of RHO-GTPase signaling and related pathways in PAH. STRING analyses demonstrated the potential importance of signaling through PKG1 and PTPRB. Notably, our findings lead to the hypothesis that tolerance to drugs which act by increasing cGMP (i.e. PDE-V inhibitors) could result from down-regulation of PKG1. Other kinase networks identified from phosphopeptide analysis revealed CSNK2A1 (casein kinase 2), CDK1, MAPK12, MAPK14, AKT1, AurkA, CamK2B, GSK3A, GSK3B, HPK2, HYRC, and PAKs as potentially important kinases in PAH. Phosphorylated IKZF3 was localized to perivascular infiltrates comprised primarily of CD3+CD8+ and CD45a+T cells. Functional assays suggested an important role of IKZF3 phosphorylation in regulating BCL2 expression. The regulated phosphopeptides and/or phosphoproteins identified in this study are candidate biomarkers for diagnosis, prognosis, or targeted therapy for PAH.

Acknowledgments

We thank Mary LoPresti, Edward Voss, and Jean Kanyo from the Keck MS & Proteomics Resource at Yale University for their sample preparation and phosphoproteomics mass spectral data collection.

Declaration of conflicting interests

The author(s) declared the following potential conflicts of interest with respect to the research, authorship, and/or publication of this

article: Sitapara and Zisman were employees of Pulmokine at the time the study was conducted, and own stock in Pulmokine Inc.

Funding

The author(s) disclosed receipt of the following financial support for the research, authorship, and/or publication of this article: RMT was supported by the grants NHLBI R24 HL123767 and NHLBI P01 HL14985. Research reported in this publication was supported by the National Heart, Lung, and Blood Institute of the National Institutes of Health under Award Number R03HL110821 to LSZ. The content is solely the responsibility of the authors and does not necessarily represent the official views of the National Institutes of Health.

Ethical approval

Exempt as per 45CFR46.

Guarantor

Lawrence S Zisman.

Authors' contributions

Substantial contributions to the conception or design of the work, or the acquisition, analysis, or interpretation of data for the work: Ravikumar Sitapara, TuKiet T Lam, Aneta Gandjeva, Rubin M Tuder, and Lawrence S Zisman. Drafting the work or revising it critically for important intellectual content: Ravikumar Sitapara, TuKiet T Lam, Aneta Gandjeva, Rubin M Tuder, and Lawrence S Zisman. Final approval of the version to be published: Ravikumar Sitapara, TuKiet T Lam, Aneta Gandjeva, Rubin M Tuder, and Lawrence S Zisman. Agreement to be accountable for all aspects of the work in ensuring that questions related to the accuracy or integrity of any part of the work are appropriately investigated and resolved: Ravikumar Sitapara, TuKiet T Lam, Aneta Gandjeva, Rubin M Tuder, and Lawrence S Zisman.

ORCID iD

Lawrence S. Zisman  <https://orcid.org/0000-0002-7975-4707>

References

1. Edwards WD and Edwards JE. Clinical primary pulmonary hypertension: three pathologic types. *Circulation* 1977; 56: 884–888.
2. Fishman AP. Changing concepts of the pulmonary plexiform lesion. *Physiol Res* 2000; 49: 485–492.
3. Hsieh SP, Wang JS, Tsui CY, et al. Plexogenic pulmonary vascular lesions in primary pulmonary arteriopathy – report of two autopsy cases. *Zhonghua Yi Xue Za Zhi* 1990; 45: 134–138.
4. Loyd JE, Atkinson JB, Pietra GG, et al. Heterogeneity of pathologic lesions in familial primary pulmonary hypertension. *Am Rev Respir Dis* 1988; 138: 952–957.
5. Ogata T and Iijima T. Structure and pathogenesis of plexiform lesion in pulmonary hypertension. *Chin Med J* 1993; 106: 45–48.
6. Tuder RM, Groves B, Badesch DB, et al. Exuberant endothelial cell growth and elements of inflammation are present in plexiform lesions of pulmonary hypertension. *Am J Pathol* 1994; 144: 275–285.

7. Tuder RM and Voelkel NF. Plexiform lesion in severe pulmonary hypertension: association with glomeruloid lesion. *Am J Pathol* 2001; 159: 382–383.
8. Bull TM, Coldren CD, Moore M, et al. Gene microarray analysis of peripheral blood cells in pulmonary arterial hypertension. *Am J Respir Crit Care Med* 2004; 170: 911–919.
9. Lavoie JR, Ormiston ML, Perez-Iratxeta C, et al. Proteomic analysis implicates translationally controlled tumor protein as a novel mediator of occlusive vascular remodeling in pulmonary arterial hypertension. *Circulation* 2014; 129: 2125–2135.
10. Meyrick BO, Friedman DB, Billheimer DD, et al. Proteomics of transformed lymphocytes from a family with familial pulmonary arterial hypertension. *Am J Respir Crit Care Med* 2008; 177: 99–107.
11. Rhodes CJ, Otero-Nunez P, Wharton J, et al. Whole blood RNA profiles associated with pulmonary arterial hypertension and clinical outcome. *Am J Respir Crit Care Med* 2020; 202: 586–594.
12. Rhodes CJ, Wharton J, Ghataorhe P, et al. Plasma proteome analysis in patients with pulmonary arterial hypertension: an observational cohort study. *Lancet Respir Med* 2017; 5: 717–726.
13. Ulrich S, Taraseviciene-Stewart L, Huber LC, et al. Peripheral blood B lymphocytes derived from patients with idiopathic pulmonary arterial hypertension express a different RNA pattern compared with healthy controls: a cross sectional study. *Respir Res* 2008; 9: 20.
14. West J, Cogan J, Geraci M, et al. Gene expression in BMPR2 mutation carriers with and without evidence of pulmonary arterial hypertension suggests pathways relevant to disease penetrance. *BMC Med Genomics* 2008; 1: 45.
15. Xu W, Comhair SAA, Chen R, et al. Integrative proteomics and phosphoproteomics in pulmonary arterial hypertension. *Sci Rep* 2019; 9: 18623.
16. Yeager ME, Colvin KL, Everett AD, et al. Plasma proteomics of differential outcome to long-term therapy in children with idiopathic pulmonary arterial hypertension. *Proteomics Clin Appl* 2012; 6: 257–267.
17. Stearman RS, Bui QM, Speyer G, et al. Systems analysis of the human pulmonary arterial hypertension lung transcriptome. *Am J Respir Cell Mol Biol* 2019; 60: 637–649.
18. Saygin D, Tabib T, Bittar HET, et al. Transcriptional profiling of lung cell populations in idiopathic pulmonary arterial hypertension. *Pulm Circ* 2020; 10: 1–15.
19. Rhodes CJ, Im H, Cao A, et al. RNA sequencing analysis detection of a novel pathway of endothelial dysfunction in pulmonary arterial hypertension. *Am J Respir Crit Care Med* 2015; 192: 356–366.
20. Antoniu SA. Targeting RhoA/ROCK pathway in pulmonary arterial hypertension. *Expert Opin Ther Targets* 2012; 16: 355–363.
21. Barst RJ. PDGF signaling in pulmonary arterial hypertension. *J Clin Invest* 2005; 115: 2691–2694.
22. Chhina MK, Nargues W, Grant GM, et al. Evaluation of imatinib mesylate in the treatment of pulmonary arterial hypertension. *Future Cardiol* 2010; 6: 19–35.
23. Dempsey EC, McMurtry IF and O'Brien RF. Protein kinase C activation allows pulmonary artery smooth muscle cells to proliferate to hypoxia. *Am J Physiol* 1991; 260: L136–L145.
24. Doggrel SA. Rho-kinase inhibitors show promise in pulmonary hypertension. *Expert Opin Investig Drugs* 2005; 14: 1157–1159.
25. Farha S, Dweik R, Rahaghi F, et al. Imatinib in pulmonary arterial hypertension: c-Kit inhibition. *Pulm Circ* 2014; 4: 452–455.
26. Ghofrani HA, Morrell NW, Hoeper MM, et al. Imatinib in pulmonary arterial hypertension patients with inadequate response to established therapy. *Am J Respir Crit Care Med* 2010; 182: 1171–1177.
27. Gombert-Maitland M, Maitland ML, Barst RJ, et al. A dosing/cross-development study of the multikinase inhibitor sorafenib in patients with pulmonary arterial hypertension. *Clin Pharmacol Ther* 2010; 87: 303–310.
28. Jasinska-Stroschein M, Owczarek J, Plichta P, et al. Concurrent rho-kinase and tyrosine kinase platelet-derived growth factor inhibition in experimental pulmonary hypertension. *Pharmacology* 2014; 93: 145–150.
29. Ma J, Zhang L, Han W, et al. Activation of JNK/c-Jun is required for the proliferation, survival, and angiogenesis induced by EET in pulmonary artery endothelial cells. *J Lipid Res* 2012; 53: 1093–1105.
30. Medarametla V, Festin S, Sugarraghaa C, et al. PK10453, a nonselective platelet-derived growth factor receptor inhibitor, prevents the progression of pulmonary arterial hypertension. *Pulm Circ* 2014; 4: 82–102.
31. Minatsuki S, Miura I, Yao A, et al. Platelet-derived growth factor receptor-tyrosine kinase inhibitor, imatinib, is effective for treating pulmonary hypertension induced by pulmonary tumor thrombotic microangiopathy. *Int Heart J* 2015; 56: 245–248.
32. Miyagawa K and Emoto N. A new class of drug for pulmonary arterial hypertension. Can a Rho-kinase inhibitor break the stagnation in treating it? *Circ J* 2013; 77: 2477–2478.
33. Morecroft I, Doyle B, Nilsen M, et al. Mice lacking the Raf-1 kinase inhibitor protein exhibit exaggerated hypoxia-induced pulmonary hypertension. *Br J Pharmacol* 2011; 163: 948–963.
34. Ramchandran R, Raghavan A, Geenen D, et al. PKG-1alpha leucine zipper domain defect increases pulmonary vascular tone: implications in hypoxic pulmonary hypertension. *Am J Physiol Lung Cell Mol Physiol* 2014; 307: L537–L544.
35. Sakao S and Tatsumi K. Vascular remodeling in pulmonary arterial hypertension: multiple cancer-like pathways and possible treatment modalities. *Int J Cardiol* 2011; 147: 4–12.
36. Sakao S, Tatsumi K and Voelkel NF. Reversible or irreversible remodeling in pulmonary arterial hypertension. *Am J Respir Cell Mol Biol* 2010; 43: 629–634.
37. Yu L, Quinn DA, Garg HG, et al. Cyclin-dependent kinase inhibitor p27Kip1, but not p21WAF1/Cip1, is required for inhibition of hypoxia-induced pulmonary hypertension and remodeling by heparin in mice. *Circ Res* 2005; 97: 937–945.
38. Stacher E, Graham BB, Hunt JM, et al. Modern age pathology of pulmonary arterial hypertension. *Am J Respir Crit Care Med* 2012; 186: 261–272.
39. Soderblom EJ, Philipp M, Thompson JW, et al. Quantitative label-free phosphoproteomics strategy for multifaceted experimental designs. *Anal Chem* 2011; 83: 3758–3764.
40. Linding R, Jensen LJ, Ostheimer GJ, et al. Systematic discovery of in vivo phosphorylation networks. *Cell* 2007; 129: 1415–1426.

41. Linding R, Jensen LJ, Pasculescu A, et al. NetworKIN: a resource for exploring cellular phosphorylation networks. *Nucleic Acids Res* 2008; 36: D695–D699.
42. Goel RK, Meyer M, Paczkowska M, et al. Global phosphoproteomic analysis identifies SRMS-regulated secondary signaling intermediates. *Proteome Sci* 2018; 16: 16.
43. Safaei J, Manuch J, Gupta A, et al. Prediction of 492 human protein kinase substrate specificities. *Proteome Sci* 2011; 9(Suppl 1): S6.
44. Bogaard HJ, Mizuno S, Hussaini AA, et al. Suppression of histone deacetylases worsens right ventricular dysfunction after pulmonary artery banding in rats. *Am J Respir Crit Care Med* 2011; 183: 1402–1410.
45. Galletti M, Cantoni S, Zambelli F, et al. Dissecting histone deacetylase role in pulmonary arterial smooth muscle cell proliferation and migration. *Biochem Pharmacol* 2014; 91: 181–190.
46. Lan B, Hayama E, Kawaguchi N, et al. Therapeutic efficacy of valproic acid in a combined monocrotaline and chronic hypoxia rat model of severe pulmonary hypertension. *PLoS One* 2015; 10: e0117211.
47. Zhao L, Chen CN, Hajji N, et al. Histone deacetylation inhibition in pulmonary hypertension: therapeutic potential of valproic acid and suberoylanilide hydroxamic acid. *Circulation* 2012; 126: 455–467.
48. Abdul-Salam VB, Paul GA, Ali JO, et al. Identification of plasma protein biomarkers associated with idiopathic pulmonary arterial hypertension. *Proteomics* 2006; 6: 2286–2294.
49. Geraci M and Meyrick B. Genomics and proteomics of pulmonary vascular disease. *Compr Physiol* 2011; 1: 467–483.
50. Abdul-Salam VB, Wharton J, Cupitt J, et al. Proteomic analysis of lung tissues from patients with pulmonary arterial hypertension. *Circulation* 2010; 122: 2058–2067.
51. Ohata Y, Ogata S, Nakanishi K, et al. Proteomic analysis of the lung in rats with hypobaric hypoxia-induced pulmonary hypertension. *Histol Histopathol* 2013; 28: 893–902.
52. Ostergaard L, Honore B, Thorsen LB, et al. Pulmonary pressure reduction attenuates expression of proteins identified by lung proteomic profiling in pulmonary hypertensive rats. *Proteomics* 2011; 11: 4492–4502.
53. de Kreuk BJ, Schaefer A, Anthony EC, et al. The human minor histocompatibility antigen 1 is a RhoGAP. *PLoS One* 2013; 8: e73962.
54. Johnson JA, Hemnes AR, Perrien DS, et al. Cytoskeletal defects in Bmpr2-associated pulmonary arterial hypertension. *Am J Physiol Lung Cell Mol Physiol* 2012; 302: L474–L484.
55. Gomez G, Lee JH, Veldman MB, et al. Identification of vascular and hematopoietic genes downstream of ETSRP by deep sequencing in zebrafish. *PLoS One* 2012; 7: e31658.
56. ten Freyhaus H, Dagnell M, Leuchs M, et al. Hypoxia enhances platelet-derived growth factor signaling in the pulmonary vasculature by down-regulation of protein tyrosine phosphatases. *Am J Respir Crit Care Med* 2011; 183: 1092–1102.
57. Behjati S, Tarpey PS, Sheldon H, et al. Recurrent PTPRB and PLCG1 mutations in angiosarcoma. *Nat Genet* 2014; 46: 376–379.
58. Butler T, Paul J, Europe-Finner N, et al. Role of serine-threonine phosphoprotein phosphatases in smooth muscle contractility. *Am J Physiol Cell Physiol* 2013; 304: C485–C504.
59. Ma H, He Q, Dou D, et al. Increased degradation of MYPT1 contributes to the development of tolerance to nitric oxide in porcine pulmonary artery. *Am J Physiol Lung Cell Mol Physiol* 2010; 299: L117–L123.
60. Schwappacher R, Kilic A, Kojonazarov B, et al. A molecular mechanism for therapeutic effects of cGMP-elevating agents in pulmonary arterial hypertension. *J Biol Chem* 2013; 288: 16557–16566.
61. Sklepkiwicz P, Schermuly RT, Tian X, et al. Glycogen synthase kinase 3beta contributes to proliferation of arterial smooth muscle cells in pulmonary hypertension. *PLoS One* 2011; 6: e18883.
62. Takahashi J, Orcholski M, Yuan K, et al. PDGF-dependent beta-catenin activation is associated with abnormal pulmonary artery smooth muscle cell proliferation in pulmonary arterial hypertension. *FEBS Lett* 2016; 590: 101–109.
63. Kioussis D. Aiolos: an ungrateful member of the Ikaros family. *Immunity* 2007; 26: 275–277.
64. Rebollo A and Schmitt C. Ikaros, Aiolos and Helios: transcription regulators and lymphoid malignancies. *Immunol Cell Biol* 2003; 81: 171–175.
65. Schmitt C, Tonnelle C, Dalloul A, et al. Aiolos and Ikaros: regulators of lymphocyte development, homeostasis and lymphoproliferation. *Apoptosis* 2002; 7: 277–284.
66. Kim J, Sif S, Jones B, et al. Ikaros DNA-binding proteins direct formation of chromatin remodeling complexes in lymphocytes. *Immunity* 1999; 10: 345–355.
67. Hosokawa Y, Maeda Y, Takahashi E, et al. Human aiolos, an ikaros-related zinc finger DNA binding protein: cDNA cloning, tissue expression pattern, and chromosomal mapping. *Genomics* 1999; 61: 326–329.
68. Cortes M, Wong E, Koipally J, et al. Control of lymphocyte development by the Ikaros gene family. *Curr Opin Immunol* 1999; 11: 167–171.
69. Wang JH, Avitahl N, Cariappa A, et al. Aiolos regulates B cell activation and maturation to effector state. *Immunity* 1998; 9: 543–553.
70. Kelley CM, Ikeda T, Koipally J, et al. Helios, a novel dimerization partner of Ikaros expressed in the earliest hematopoietic progenitors. *Curr Biol* 1998; 8: 508–515.
71. Morgan B, Sun L, Avitahl N, et al. Aiolos, a lymphoid restricted transcription factor that interacts with Ikaros to regulate lymphocyte differentiation. *EMBO J* 1997; 16: 2004–2013.
72. Georgopoulos K, Winandy S and Avitahl N. The role of the Ikaros gene in lymphocyte development and homeostasis. *Annu Rev Immunol* 1997; 15: 155–176.
73. Licht JD, Shortt J and Johnstone R. From anecdote to targeted therapy: the curious case of thalidomide in multiple myeloma. *Cancer Cell* 2014; 25: 9–11.
74. Billot K, Parizot C, Arrouss I, et al. Differential aiolos expression in human hematopoietic subpopulations. *Leuk Res* 2010; 34: 289–293.
75. Duhamel M, Arrouss I, Merle-Beral H, et al. The Aiolos transcription factor is up-regulated in chronic lymphocytic leukaemia. *Blood* 2008; 111: 3225–3228.
76. Antica M, Cicin-Sain L, Kapitanovic S, et al. Aberrant Ikaros, Aiolos, and Helios expression in Hodgkin and non-Hodgkin lymphoma. *Blood* 2008; 111: 3296–3297.
77. Holmes ML, Huntington ND, Thong RP, et al. Peripheral natural killer cell maturation depends on the transcription factor Aiolos. *Embo J* 2014; 33: 2721–2734.

78. Zhuang Y, Lu Y, Li D, et al. Upregulation of AIOLOS induces apoptosis and enhances etoposide chemosensitivity in Jurkat leukemia cells. *Oncol Rep* 2015; 33: 1319–1325.
79. Zhuang Y, Li D, Fu J, et al. Overexpression of AIOLOS inhibits cell proliferation and suppresses apoptosis in Nalm-6 cells. *Oncol Rep* 2014; 31: 1183–1190.
80. Wang R, Guo G, Li H, et al. Overexpression of Aiolos in Nalm-6 acute lymphoblastic leukaemia cells reduces apoptosis by suppressing phosphatase and tensin homologue deleted on chromosome 10 and activating the phosphatidylinositol-3-kinase/Akt signalling pathway. *Mol Med Rep* 2015; 11: 3457–3464.
81. Kikuchi H, Yamashita K, Nakayama M, et al. Lacking of Aiolos accelerates pre-mature B cell apoptosis mediated by BCR signaling through elevation in cytochrome c release. *Biochim Biophys Acta* 2009; 1793: 1304–1314.
82. Gandhi R, Kumar D, Burns EJ, et al. Activation of the aryl hydrocarbon receptor induces human type 1 regulatory T cell-like and Foxp3(+) regulatory T cells. *Nat Immunol* 2010; 11: 846–853.
83. Perros F, Dorfmuller P, Montani D, et al. Pulmonary lymphoid neogenesis in idiopathic pulmonary arterial hypertension. *Am J Respir Crit Care Med* 2012; 185: 311–321.
84. Edwards AL, Gunningham SP, Clare GC, et al. Professional killer cell deficiencies and decreased survival in pulmonary arterial hypertension. *Respirology* 2013; 18: 1271–1277.
85. Austin ED, Rock MT, Mosse CA, et al. T lymphocyte subset abnormalities in the blood and lung in pulmonary arterial hypertension. *Respir Med* 2010; 104: 454–462.
86. Benza RL, Williams G, Wu C, et al. In situ expression of Bcl-2 in pulmonary artery endothelial cells associates with pulmonary arterial hypertension relative to heart failure with preserved ejection fraction. *Pulm Circ* 2016; 6: 551–556.
87. Perros F, Sentenac P, Boulate D, et al. Smooth muscle phenotype in idiopathic pulmonary hypertension: hyperproliferative but not cancerous. *Int J Mol Sci* 2019; 20: 3575.
88. Chowdhury HM, Sharmin N, Yuzbasioglu Baran M, et al. BMPRII deficiency impairs apoptosis via the BMPRII-ALK1-BclX-mediated pathway in pulmonary arterial hypertension. *Hum Mol Genet* 2019; 28: 2161–2173.